JOURNAL OF SOLID STATE CHEMISTRY 137, 249–254 (1998)
ARTICLE NO. SC977723

Spin-Glass-like Behavior in the Selenide $Cr_2Sn_3Se_7$

F. Bodénan, V. B. Cajipe,[1] M. Danot, and G. Ouvrard

Institut des Matériaux de Nantes, Laboratoire de Chimie des Solides, UMR 6502, 2 rue de la Houssinière, BP 32229, 44322 Nantes Cedex 3, France

Received June 23, 1997; in revised form November 23, 1997; accepted December 4, 1997

Magnetic measurements show that monoclinic $Cr_2Sn_3Se_7$ exhibits many of the defining characteristics of a spin glass below 30 K. Low-temperature ^{119}Sn Mössbauer spectroscopy and neutron powder diffraction data are also consistent with the occurrence of short-range magnetic order. This behavior is discussed in relation to the probable nature of magnetic interactions and the origin of randomness in $Cr_2Sn_3Se_7$. © 1998 Academic Press

Key Words: **chromium selenide; spin glass; ^{119}Sn Mössbauer spectroscopy.**

INTRODUCTION

Within the past 15 years the study of spin glass behavior, first detected in dilute metallic alloys, has been extended to a large number of more concentrated and nonmetallic systems. The occurrence of a transition in which spin orientations freeze without establishing long-range order requires that the magnetic sublattice exhibit a high degree of randomness and the spins be subject to strongly competing interactions. These conditions are satisfied in some amorphous compounds. More typically, however, spin glass or other frozen spin behavior has been observed in materials with crystalline structures characterized by some combination of magnetic site disorder and a geometry favoring frustration (1).

Recently, our search for ternary chromium chalcogenides containing low-dimensional magnetic sublattices led to the synthesis and the structural characterization of a new selenide with the formula $Cr_2Sn_3Se_7$($Cr_2^{III}Sn^{II}Sn_2^{IV}Se_7$). There are two variants of this compound, one with a monoclinic (space group $P2_1/m$) (2) and the other with an orthorhombic (*Pnma*) [3] structure. Each may be described in terms of edge-sharing selenium octahedra forming $[M_2Se_6]$ ribbons and $[MSe_2]$ sheets as shown in Fig. 1a for the monoclinic phase ($a = 12.765(5)$ Å, $b = 3.835(2)$ Å, and $c = 11.785(4)$ Å, $\beta = 105.21^\circ$). The octahedral sites M form a triangular network and are statistically occupied by the magnetic Cr^{III} and diamagnetic Sn^{IV} cations in a 2 : 1 ratio (Fig. 1b); the tunnels defined by the sheets and ribbons are filled by the Sn^{II}.

[1] To whom correspondence should be addressed.

Initial dc magnetic susceptibility measurements revealed a maximum in the 20–30 K range for both forms of $Cr_2Sn_3Se_7$ (2, 3). This feature was found to be sensitive to whether cooling is done with or without an applied field. Moreover, the temperature at which this maximum appears in the orthorhombic phase was shown to be field-dependent. Such observations are consistent with a freezing in of magnetic disorder and a low-temperature superparamagnetic or spin glass state has been suggested for these selenides [3].

In this paper, we present results of new magnetic measurements as well as ^{119}Sn Mössbauer spectroscopy and neutron diffraction experiments performed on monoclinic $Cr_2Sn_3Se_7$. The data are discussed in relation to the peculiarities of the Cr^{III} sublattice and the hypothesis of spin glass behavior.

EXPERIMENTAL

Monoclinic $Cr_2Sn_3Se_7$ was prepared via solid-state reaction as previously described (2). Dc magnetic measurements were carried out using a Quantum Design SQUID magnetometer on two samples: 13 mg of selected needlelike crystals and 60 mg of powder sieved to 20 μm and verified pure by X-ray diffraction and scanning electron microscopy analysis of polished sections. Ac magnetic susceptibility measurements were performed with a Lakeshore susceptometer on 100 mg of the powder sieved to 20 μm. ^{119}Sn Mössbauer spectra were obtained with a constant-acceleration spectrometer using a symmetric sawtooth vibrator; isomer shifts were measured relative to $CaSnO_3$ at 300 K. Neutron diffraction experiments were carried out on the G4.1 multidetector powder diffractometer at the Laboratoire Léon Brillouin (CEA-Saclay, France) using 5 g of powder sieved to 100 μm; data were collected with $\lambda = 2.422$ Å at $5 < 2\theta < 85^\circ$ and in 0.1° steps.

RESULTS

Magnetic Measurements

The thermal evolution of the inverse dc magnetic susceptibility of monoclinic $Cr_2Sn_3Se_7$, corrected for diamagnetism,

0022-4596/98 $25.00

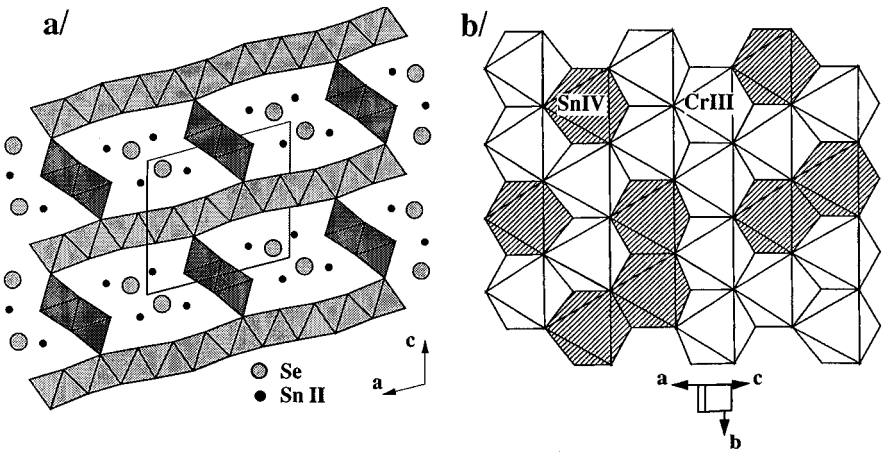

FIG. 1. (a) Projection along the *b* axis of the monoclinic structure of $Cr_2Sn_3Se_7$ showing how edge-sharing selenium octahedra form $[MSe_2]$ sheets in the (*ab*) plane connected by double rutile chains or $[M_2Se_6]$, ribbons. *M* corresponds to $\frac{2}{3}Cr^{III}$ and $\frac{1}{3}Sn^{IV}$. The black dots (gray circles) in the intervening voids represent Sn^{II} (Se). (b) Projection onto the $[MSe_2]$ sheet showing the triangular network of octahedral sites statistically occupied by Cr^{III} and Sn^{IV}.

is displayed in Fig. 2a. At $T > 150$ K, χ^{-1} follows a Curie–Weiss law with $\mu_{eff} = 4.04(1)\ \mu_B$, and $\Theta_p = 16(1)$ K. The former value confirms the trivalent state of the chromium cations, while the latter signals a weak predominance of ferromagnetic interactions in the paramagnetic regime. Deviation from Curie–Weiss behavior is evident just below 150 K, signifying the onset of magnetic correlations at fairly high temperatures. These presumably develop with cooling and give rise to the transition at $T < 30$ K.

Figure 2b shows the low-temperature dc magnetic susceptibility χ measured upon warming after zero-field cooling or field cooling (ZFC or FC, respectively) and at various values of the applied field *H*. The FC and ZFC curves measured at 500 G are clearly distinguishable. Zero-field cooling yields a susceptibility maximum around 20 K, while field cooling leads to weakly increasing χ values below this temperature. This difference may be ascribed to distinct ways of freezing the spins: in random directions under ZFC and aligned with the applied field during FC. The peak in the ZFC curve indicates the temperature T_f at which the spins freeze. This maximum becomes rounder and depressed in magnitude at stronger fields, while T_f decreases. At higher field values, enough magnetic energy is available for spins to overcome the energy barrier (the freezing temperature) separating various possible states of randomly oriented moments. Magnetic irreversibility thus diminishes with increasing field. These results accord with the occurrence of low-temperature magnetic disorder (4) as observed in spin glass, superparamagnetic, or fine-particle systems (5).

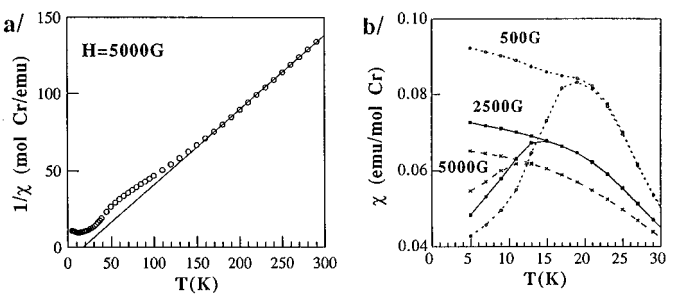

FIG. 2. (a) Inverse dc magnetic susceptibility χ^{-1} measured under zero-field-cooling (ZFC) conditions and with $H = 5$ kG; the solid line represents the Curie–Weiss fit to the data. (b) dc magnetic susceptibility χ versus temperature in the 5–30 K range for various fields and after ZFC and FC (field cooling).

The in-phase (χ') and out-of-phase (χ'') components of the ac magnetic susceptibility were measured simultaneously between 5 and 50 K in the 25- to 1000-Hz frequency range at small fields (1.2–10.0 G). For a given frequency, no field dependence was found in the thermal evolution of χ' and χ''. Figure 3a displays typical curves measured at 7.5 G and various frequencies. At $T > 40$ K, the χ' curves at different frequencies superpose perfectly and χ'' is zero, signifying thermodynamic equilibrium in this higher temperature range (6). Broad maxima appear in both χ' and χ'' around 28 K, i.e., at a T_f' and T_f'' greater than the static T_f as may be expected given the low measuring fields. The width of the χ'' curve may be atributed to a distribution of relaxation times near the freezing temperature. Noting that local arrangements or "clusters" of Cr^{III} moments most probably exist in $Cr_2Sn_3Se_7$, this suggests that intercluster interactions occur (6).

A sensitivity of T_f' to the measuring frequency is evident in Figs. 3a and 3b. T_f' for each frequency was determined by taking the derivative of χ'. The values are gathered in Table 1, with errors deduced from the field independence of T_f'. The χ' maximum shifts to higher temperatures with increasing frequency but is constant between 667 and

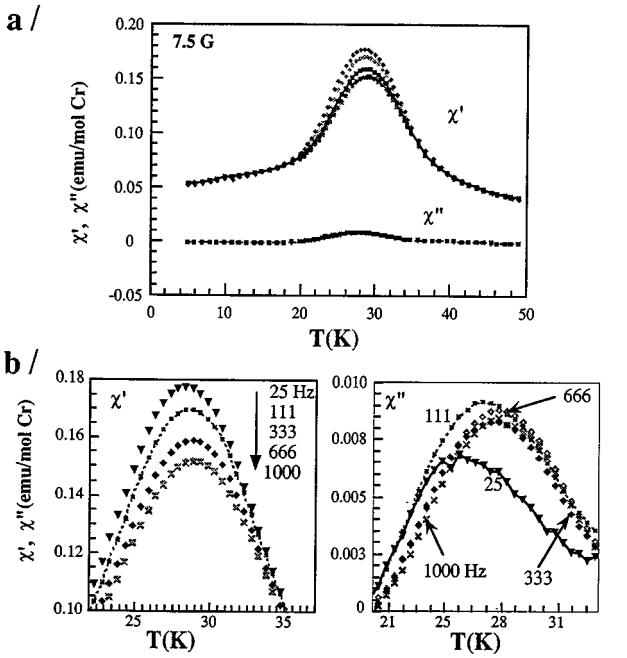

FIG. 3. (a) ac magnetic susceptibility (χ' and χ'') versus temperature in the 5–50 K range for an applied field of 7.5 G and various frequencies. (b) Details of the frequency dependence of χ' and χ''.

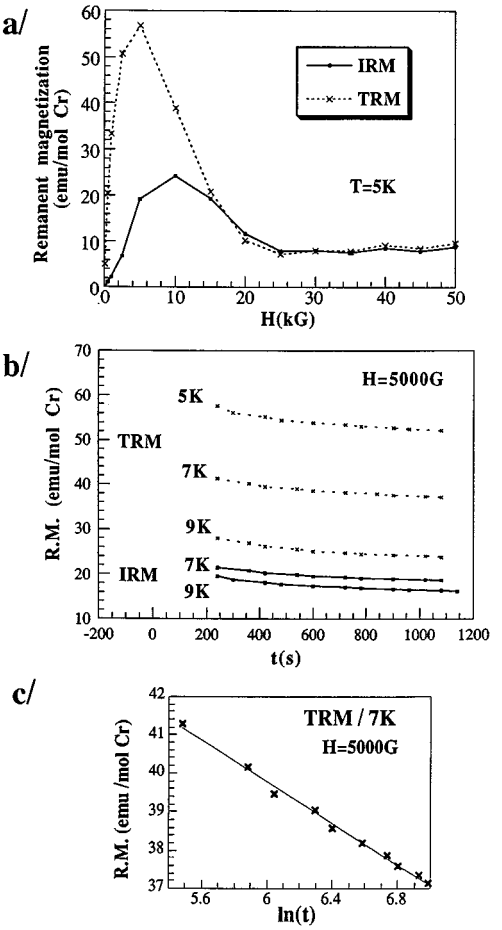

FIG. 4. (a) Field dependence of the thermoremanent (TRM) and the isothermal remanent magnetization (IRM) at 5 K. (b) Time dependence of the TRM and IRM at H = 5000G for various $T < T_f$. (c) Logarithmic fit for decay of TRM at 7 K.

1000 Hz, i.e., when the field is applied for 1.5×10^{-3} s or less. The frequency shift of T_f' per decade ν, $\Delta T_f'/[T_f' \log(\Delta\nu)]$, has been used as an empirical criterion to distinguish spin glasses and spin-glass-like materials from superparamagnets (7). Indeed, this quantity obtained for $\nu = 667$Hz is of the order 10^{-2} in $Cr_2Sn_3Se_7$ which is quite similar to values found for spin glass systems. T_f'' also has some frequency-dependence which proved difficult to specify because its value could not be unambiguously extracted from the χ'' derivative calculated at each measuring frequency. For the less noisy curve at 1000 Hz, however, a $T_f'' = 27.5(3)$ K could be determined, i.e., $T_f'' \neq T_f'$. This inequality associated with the frequency dependence of both χ' and χ'' has been cited as an exact criterion for spin glass behavior (8).

A nonzero χ'' at low temperature ($20 < T < 35$ K) points to the existence of remanence. The thermoremanent magnetization (TRM) and isothermal remanent magnetization (IRM) were thus measured versus temperature, field, and time. To obtain the TRM, the sample is cooled far below the freezing temperature (to 5 K) in the presence of a given field; the field is then switched off. For the IRM, the sample is cooled without a field; when the measuring temperature is reached, the field is applied for 5 min and then switched off. In both cases, measurement of the magnetization after the field was turned off took $t_0 = 30$ s.

TABLE 1
Frequency Dependence of T_f'

ν (Hz)	25	111	333	667	1000
T_f' (K)	28.07(2)	28.38(7)	28.53(4)	28.63(2)	28.66(4)

The TRM and IRM at 5 K and various applied field values are displayed in Fig. 4a. The two curves evolve with field in ways resembling those found for spin glass and superparamagnetic materials (9). Particularly, the TRM response is stronger than the IRM below a field of 15 kG. This field is referred to as the critical field H_c for the onset of irreversibility on a time scale t_0 at a given T. Usually in spin glasses, the TRM follows a linear variation at low fields and then reaches a maximum which may overshoot the saturation value at above-critical fields; the IRM approaches the critical value monotonically. For $Cr_2Sn_3Se_7$ (Fig. 4a), both the TRM and IRM exhibit a maximum. The TRM peak at $H_{max}(\text{TRM}) = 5$ kG is rather sharp, while that of the IRM around 10 kG is rounder. Also, saturation in Fig. 4a occurs above the critical field at a value significantly lower than the

TRM or IRM at H_c. Similar features have been observed in $LaCrS_3$ for which the TRM maximum has been interpreted as resulting from a rearrangement of moments in a local demagnetizing field due to moments aligned with an applied field exceeding H_{max}(TRM) (10).

The evolution with time of the remanent magnetization for an applied field of 5 kG and different $T < T_f$ is displayed in Fig. 4b. Both the TRM and IRM decay very slowly. For large fields and temperatures sufficiently below freezing, such decay as encountered in spin glasses may be described by a logarithmic law: the remanent magnetization $\sigma_R(t) = 1 - a(T,H)\ln t$, where $a(T,H)$ is related to the "magnetic viscosity" (1, 11). Figure 4c shows that this logarithmic law provides a satisfactory fit for TRM data at 7 K. The remanent magnetization decrease observed in Fig. 4b as T approaches T_f is likewise typical of spin glasses.

Another manifestation of magnetic irreversibility is the existence of hysteresis phenomena. Figure 5 shows that magnetic hysteresis indeed occurs in $Cr_2Sn_3Se_7$. The full loop obtained at 5 K (Fig. 5a) indicates that saturation is not reached at 50kG: the magnetization there is only $\approx 10\%$ of the value expected for Cr^{III}. Inspection of the low-field section of the cycle reveals the weak remanence and coercive field present in the material. The loop measured at 10 K (Fig. 5b) is narrower and remains confined within that at 5 K (weaker remanent magnetization and coercive field). A wide variety of hysteresis-cycle shapes has been found in spin glasses and superparamagnets (1). However, the smoothness and thermal variation observed in Fig. 5 appear to be consistent with the characteristics of a hysteresis loop predicted by a general model (distribution of thermally activated double-well potentials) in the spin glass rather than the superparamagnetic case (12).

^{119}*Sn Mössbauer Spectroscopy and Neutron Diffraction*

^{119}Sn Mössbauer spectroscopy measurements were first performed in the 80–296 K range to confirm the valences of the tin ions and obtain a reference spectrum for the paramagnetic state. Figure 6a shows the spectra for $T = 296$ and 80 K. Two resonances are found: one with isomer shift $\delta = 3.40(3)$ mm/s for Sn^{II}, and the other with $\delta = 1.46(3)$ mm/s for Sn^{IV}, as determined by performing Lorentzian lineshape fits to the data (Table 2). The δ values are as expected for tin ions in a selenium environment. Δ found for Sn^{II} here is weaker than for low-coordination geometries where the lone pair would be stereochemically active, thus agreeing with the trigonal prismatic coordination revealed by diffraction. The relative areas of the two resonances reflect both the Sn^{IV}/Sn^{II} ratio and the recoil-free fractions for each cation, the latter quantity being T-dependent. Figure 6b plots the logarithm of the integrated absorption,

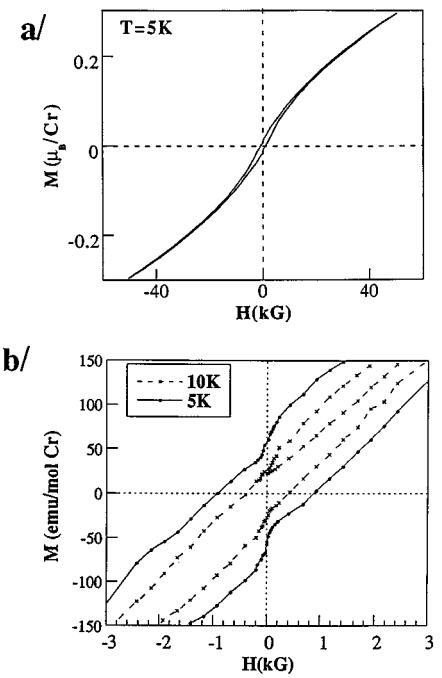

FIG. 5. (a) Full hysteresis cycle at 5 K. (b) Low-field section of loops at 5 and 10 K; for clarity, the first magnetization curve for the loop at 5 K is not shown.

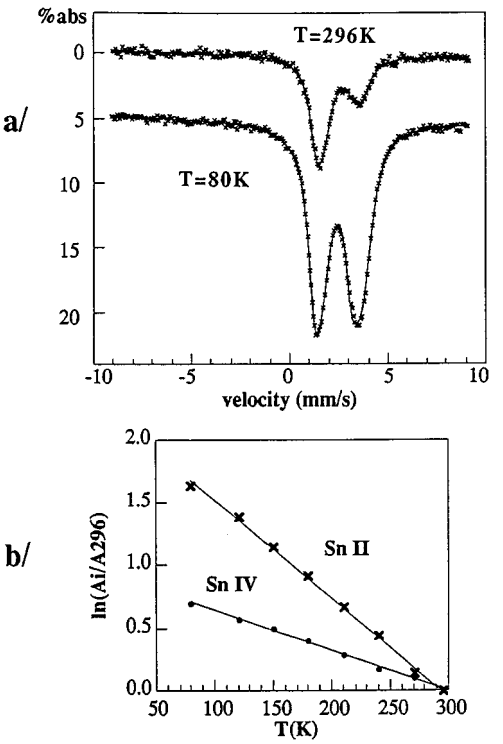

FIG. 6. (a) ^{119}Sn Mössbauer spectra at 296 and 80 K (shifted vertically by 5%); solid curves represent Lorentzian fits (Table 2). (b) Temperature dependence of $\ln[A(T)/A(296\text{ K})]$, where A is the integrated absorption in the paramagnetic region for the two tin states in $Cr_2Sn_3Se_7$.

TABLE 2
Lorentzian Fit Parameters to Resonances in the $T = 296$ K Mössbauer Spectrum[a]

	δ (mm/s)	Γ (mm/s)	Δ (mm/s)
Sn^{IV}	1.46(3)	0.49(3)	0.35(3)
Sn^{II}	3.40(3)	0.45(3)	0.46(3)

[a] δ is the isomer shift, Γ the half-width at half-maximum, and Δ the quadrupole splitting.

normalized to that at 296 K, versus T for each resonance. The linear thermal variation of both curves implies that the high-temperature Debye model approximation is valid, thus allowing calculation of the Mössbauer lattice temperature θ_M and an estimation of the relative fractions of the two oxidation states. The slopes of the curves in Fig. 6b yield $\theta_M(Sn^{IV}) = 234(10)$ K and $\theta_M(Sn^{II}) = 151(10)$ K, with which the respective Lamb-Mössbauer factors $f = f(T)$ may be calculated. Using the f values and the higher quality spectrum at 80 K, one obtains a Sn^{IV}/Sn^{II} ratio of 40/60, which is fairly close to the 33/67 value assumed in the structural refinement.

As the temperature is decreased through T_f, the occurrence of Zeeman hyperfine splitting becomes more evident (Fig. 7) and reflects the presence of magnetic hyperfine fields transferred from the neighboring magnetic cations to the resonant nuclei. The Sn^{IV} contribution becomes increasingly diffuse, spreading over a wide velocity range so that it

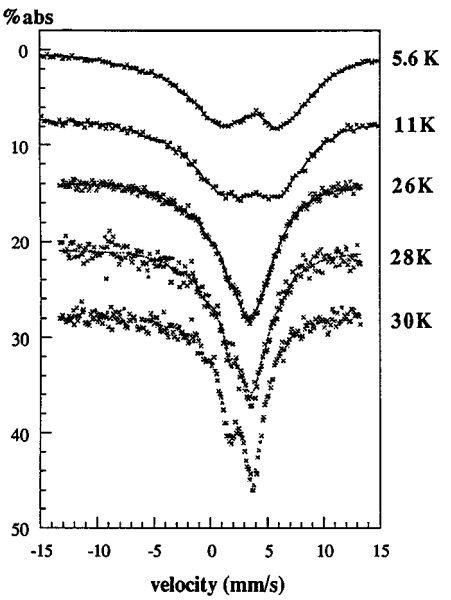

FIG. 7. ^{119}Sn Mössbauer spectra at $T = 30$ K. The 11, 26, 28, and 30 K spectra are shifted vertically from the zero baseline.

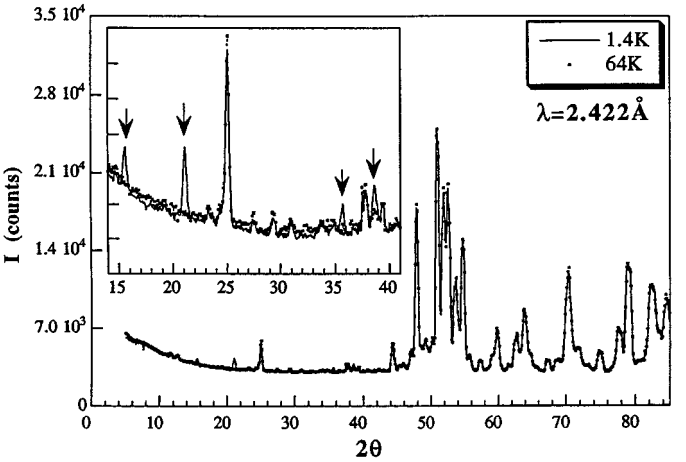

FIG. 8. Neutron powder diffraction patterns at 1.4 and 64 K. Inset shows small magnetic contributions due to the impurity Cr_2Se_3.

becomes hardly observable in the spectra recorded at the lowest temperatures. This implies a rather broad distribution of transferred fields and precludes proposing a meaningful quantitative description for this contribution. The Sn^{II} singlet transforms with cooling into a broadened doublet ascribable to an unresolved magnetic contribution which also reflects the presence of a field distribution. In this case, the average field value may be estimated to be 40–50 kG at 5.6 K. The distributions may be attributed to the existence of different magnetic environments around the tin nuclei, which in turn is due to the cationic site disorder and the freezing of randomly oriented Cr^{III} moments. Similar observations have been made in Mössbauer spectra of spin glasses as well as superparamagnetic and fine-particle systems (13).

Clusters of correlated frozen spins, if large enough (>10 Å), should lead to the appearance of diffuse scattering in a neutron powder diffraction pattern (14). Diffractograms were thus recorded for $Cr_2Sn_3Se_7$ at 64 and 1.4 K as shown in Fig. 8. Additional peaks that index according to the known antiferromagnetic phase of Cr_2Se_3 (15) are observed at 1.4 K ($T_N = 45$ K); the presence of this impurity, which is difficult to avoid in preparing a 5-g sample, was confirmed by analysis of a polished section. Aside from this, a comparison of the two patterns does not reveal any magnetic scattering at 1.4 K. This implies that the Cr^{III} clusters in $Cr_2Sn_3Se_7$ are too small to be detected by this technique.

CONCLUSION

Our measurements have shown that $Cr_2Sn_3Se_7$ indeed exhibits many of the defining characteristics of a spin glass. How the structure of this selenide supports short-range magnetic order merits some comment.

The nearest-neighbor (nn) Cr–Cr distance within an $[MSe_2]$ sheet takes on one of four values in the 3.685- to 3.835-Å range; within an $[M_2Se_6]$ ribbon, d_{Cr-Cr} is either 3.831 or 3.835Å (2). These are too large for direct exchange to prevail, so the nn interactions should be of the superexchange type (via the Se orbitals) (14, 16). Given that the Cr–Se–Cr angles here are close to 90°, one would expect the coupling to be ferromagnetic, in agreement with the positive Θ_p deduced from Figure 2a. A correlation established between the sign of the interaction and the nn Cr^{III} distance in various sulfides and selenides accords with this statement (13). In $CrSbSe_3$, which contains $[Cr_2Se_6]$ ribbons and is ferromagnetic below 72 K, stronger (weaker) ferromagnetic coupling is associated with the longer 3.775-Å (shorter 3.604 Å) Cr–Cr distance (17). A similar dependence on Cr–Cr distance may be assumed valid for the coupling strength in $Cr_2Sn_3Se_7$, which would then be greatest where $d_{Cr-Cr} = 3.835$ Å (parallel to the b axis within a sheet). Because the nn interactions are ferro- rather than antiferromagnetic, the presence of triangular M motifs may not be said to lead to topological frustration in the present case. On the other hand, the phenomena observed herein might be related to a model system in which ferromagnetic order competes with spin glass behavior and a percolation threshold exists (1, 18).

Inhibition of long-range magnetic order in $Cr_2Sn_3Se_7$ is clearly a consequence of the $2Cr^{III}:Sn^{IV}$ site disorder. That Cr^{III} and Sn^{IV} statistically occupy the octahedral sites rather than segregate into $[CrSe_2]$ and $[Sn_2Se_6]$ entities (19), follows from the small difference between the Cr^{III} and Sn^{IV} radii ($\Delta = 0.085$ Å). The anisotropies of the M (Cr^{III} or Sn^{IV}) sublattice also play a key role in determining the magnetic behavior. Extended ferromagnetic order in an $[MSe_2]$ sheet is foiled by the random presence of Sn^{IV}: clusters of ferromagnetically coupled Cr^{III} moments thus probably form, with distortions of the ferromagnetic state occurring close to the dilution sites. Because two-thirds of the M sites are occupied by Cr^{III}, these clusters would not be isolated from one another and should interact. Intercluster coupling within a sheet could be randomly ferro- or antiferromagnetic. Further, interactions with the disordered M sublattice of adjacent $[M_2Se_6]$ ribbons could provide another element of randomness. The ribbons attach to either face of a sheet with a periodicity of $a/2$. Intrasheet order parallel to the b axis would moreover be disrupted by site disorder along the ribbon. A cluster within a sheet would conceivably be not much bigger than $b \times a/2$, thus explaining the nondetection of diffuse scattering in the neutron experiment.

In conclusion, our measurements have shown that $Cr_2Sn_3Se_7$ indeed exhibits many of the defining characteristics of a spin glass. While dilution remains the primary cause of randomness, the probable predominance of ferromagnetic interactions and the peculiar anisotropies of the magnetic sublattice in $Cr_2Sn_3Se_7$ set it apart from most spin glass systems.

ACKNOWLEDGMENTS

We thank Y. Moëlo for help in preparing and inspecting the polished sections, G. André for assistance during the neutron diffraction experiments, and S. Maingaud for help with the Mössbauer spectroscopy measurements.

REFERENCES

1. K. Binder and A. P. Young, *Rev. Mod. Phys.* **58,** 4 (1986).
2. S. Jobic, P. Le Boterf, R. Brec, and G. Ouvrard, *J. Alloys Compd.* **205,** 139 (1994).
3. S. Jobic, F. Bodénan, G. Ouvrard, E. Elkaim, and J. P. Lauriat, *J. Solid State Chem.* **115,** 165 (1995).
4. J. L. Dormann and M. Noguès, *Phase Transitions* **33,** 159 (1991).
5. M. El-Hilo, K. O'Grady and R. W. Chantrell, *J. Magn. Magn. Mater.* **114,** 307 (1992).
6. D. Hüser, L. E. Wenger, A. J. Van Duyneveldt, and J. A. Mydosh, *Phys. Rev. B* **27**, 3100 (1983).
7. J. A. Mydosh, *in* "Spin Glasses," p. 66. Taylor and Francis, London, 1993.
8. S. L. Suib and L. E. Iton, *Chem. Mater.* **6,** 429 (1994).
9. (a) J. L. Tholence and R. Tournier, *J. Phys. Colloq.* **C4,** 4 (1974); (b) H. Maletta and W. Felsch, *Phys. Rev. B* **20,** 1245 (1979).
10. A. Lafond, A. Meerschaut, J. Rouxel, J. L. Tholence and A. Sulpice, *Phys. Rev. B* **52**, 2 (1995).
11. J. Ferré, J. Rajchenbach, and H. Maletta, *J. Appl. Phys.* **52,** 1697 (1981).
12. J. Souletie, *J. Phys.* **44,** 1095 (1983).
13. P. Colombet and M. Danot, *Solid State Commun.* **45,** 311 (1983), and references therein.
14. P. Colombet, M. Danot, and J. L. Soubeyroux, *J. Magn. Magn. Mater.* **51,** 257 (1981).
15. Y. Adachi, M. Ohashi, T. Kaneko, and M. Yuzuri, *J. Phys. Soc. Jpn.* **63,** 1548 (1994).
16. J. B. Goodenough, "Magnetism and the Chemical Bond." Wiley-Interscience, New York, 1963.
17. D. A. Odink, V. Carteaux, C. Payen, and G. Ouvrard, *Chem. Mater.* **5,** 237 (1993).
18. M. V. Simkin, *Phys. Rev. B* **55,** 11405 (1997), and references therein.
19. Distinct $[InS_2]$ and $[Sn_2S_6]$ entities do exist in $In_2Sn_3S_7$. See C. Adenis, J. Olivier-Fourcade, J. C. Jumas, and E. Philippot, *Rev. Chim. Min.* **23,** 735 (1986).